Cerebral Cortex October 2007;17:2407-2419
doi:10.1093/cercor/bhl149
Advance Access publication January 4, 2007

Small-World Anatomical Networks in the Human Brain Revealed by Cortical Thickness from MRI

Yong He, Zhang J. Chen and Alan C. Evans

McConnell Brain Imaging Centre, Montreal Neurological Institute, McGill University, Montreal, QC, Canada H3A 2B4

An important issue in neuroscience is the characterization for the underlying architectures of complex brain networks. However, little is known about the network of anatomical connections in the human brain. Here, we investigated large-scale anatomical connection patterns of the human cerebral cortex using cortical thickness measurements from magnetic resonance images. Two areas were considered anatomically connected if they showed statistically significant correlations in cortical thickness and we constructed the network of such connections using 124 brains from the International Consortium for Brain Mapping database. Significant short- and long-range connections were found in both intra- and interhemispheric regions, many of which were consistent with known neuroanatomical pathways measured by human diffusion imaging. More importantly, we showed that the human brain anatomical network had robust small-world properties with cohesive neighborhoods and short mean distances between regions that were insensitive to the selection of correlation thresholds. Additionally, we also found that this network and the probability of finding a connection between 2 regions for a given anatomical distance had both exponentially truncated power-law distributions. Our results demonstrated the basic organizational principles for the anatomical network in the human brain compatible with previous functional networks studies, which provides important implications of how functional brain states originate from their structural underpinnings. To our knowledge, this study provides the first report of small-world properties and degree distribution of anatomical networks in the human brain using cortical thickness measurements.

Keywords: anatomy, connectivity, cortical thickness, magnetic resonance imaging, morphometry, scale free, small world

Introduction

The human brain is a large, interacting, complex network with nontrivial topological properties (Sporns et al. 2004; Stam 2004; Eguiluz et al. 2005; Salvador, Suckling, Coleman, et al. 2005; Achard et al. 2006; Stam et al. 2007). The characterization for the underlying architectures of such a network is an important issue in neuroscience. It can reveal general principles of structural and functional organization in the human brain and increase our understanding of how the human brain is capable of generating and integrating information from multiple sources in real time (Sporns et al. 2004).

Thus far, most studies of complex brain networks in human have focused upon exploring connectivity patterns under functional brain states. For example, recent electroencephalogram (EEG) (Micheloyannis et al. 2006; Stam et al. 2007), magnetoencephalographic (MEG) recordings (Stam 2004) and functional magnetic resonance imaging (fMRI) (Eguiluz et al. 2005; Salvador, Suckling, Coleman, et al. 2005; Achard et al. 2006) studies have consistently demonstrated that human brain functional networks during behavior or even at resting state have the small-world property, a prominent feature shared by various social, economic, and biological networks (for a review, see Strogatz 2001). A small-world architecture indicates that the minimum path length between any pair of nodes is approximately equivalent to a comparable random network but the nodes of the network have greater local interconnectivity or cliquishness than a random network (Watts and Strogatz 1998). In addition to the small-world features, Eguiluz et al. (2005) demonstrated that human brain functional networks derived from experimentally activated fMRI data at a mesoscale (voxel level) have a scale-free power-law connection degree distribution, implying that there are a small number of regions (hubs) with an unusually large number of connections. On the other hand, another study from Achard et al. (2006) showed that functional networks of the human brain derived from resting-state fMRI data at a macroscale (regional level) follow an exponentially truncated power-law distribution, implying relatively reduced probabilities of huge hubs. The discrepancies between the connectivity degree distributions could be due to the different spatial scale analysis and/or experimental conditions of the subjects applied in the 2 studies.

Although there have been a number of studies investigating functional connectivity networks (Stam 2004; Eguiluz et al. 2005; Salvador, Suckling, Coleman, et al. 2005; Achard et al. 2006; Stam et al. 2007), little is known about the network of anatomical connections in the human brain. Definition of anatomical connectional models of the human brain is usually based on inferring knowledge from primate species such as the macaque monkey in which the connection pattern is well known (Crick and Jones 1993; Stephan et al. 2001; Penny et al. 2004). The procedure is problematic, however, partly because of our poor understanding of the evolutionary discrepancies. Direct evidence for the underlying architecture of human brain anatomical networks is still lacking (Tootell et al. 2003). Characterization of such a network would be particularly vital to reveal intrinsically structural organizational principles in the human brain and enhance our understanding of how functional brain states are associated with their structural substrates. Recently, Sporns et al. (2005) have referred to the comprehensive, detailed structural description of the network of elements and connections forming the human brain as "human connectome." There is little evidence for such an interesting but also very challenging scheme to date because of the difficulties of defining the basic structural elements of the human brain in terms of network nodes and connections (Sporns et al. 2005).

In this study, we propose an avenue of research to characterize large-scale anatomical connectivity patterns of the human

brain using morphological measurements from in vivo MRI. Cortical thickness was chosen as a morphometric feature because it reflects the size, density, and arrangement of cells (neurons, neuroglia, and nerve fibers) (Parent and Carpenter 1995; Narr et al. 2005). Particularly, 2 recent studies have suggested that interregional statistical associations in cortical thickness provide important connectivity information in the human brain (Worsley et al. 2005; Lerch et al. 2006) (we will return to this issue in the Discussion section). To study large-scale anatomical connectivity patterns in the human brain, we first segmented the entire cerebral cortex into 54 areas and automatically measured regional cortical thickness using computational neuroanatomy. Two areas were considered anatomically connected if they had significant correlations of cortical thickness across a population of 124 normal brains drawn from the International Consortium for Brain Mapping (ICBM) MRI database (Mazziotta et al. 2001). Finally, we thresholded the interregional correlation matrix to construct an undirected graph and estimated its statistical and anatomical properties, especially small-world properties and connectivity degree distribution, using graph theoretical analysis. This allows us for the first time to assess the dependencies of interregional anatomical connectivity on the anatomical relationship between regions, and to demonstrate the small-world attributes and degree distribution of human cortical networks using cortical thickness measurements from in vivo MRI.

Materials and Methods

Subjects

The subjects scanned were 152 unselected normal volunteers of the ICBM database. Each subject gave written informed consent and this study was approved by the Research Ethics Committee of the Montreal Neurological Institute and Hospital. The scans of 28 subjects were excluded from the analysis due to the left-handedness (14 subjects), unknown handedness (10 subjects), and failure of imaging processing (4 subjects). Of the remaining 124 right-handed subjects, 71 were male and 53 female. Ages ranged from 18 to 39 years (mean age 24.38, standard deviation 4.25). The characteristics of the subjects have been described previously (Watkins et al. 2001).

MRI Acquisition

MRI scans were performed on a Phillips Gyroscan 1.5-T superconducting magnet system. T_1, T_2, and proton density images were acquired for each subject with the following sequences: T_1-weighted (3D fast field echo scan with 140–160 slices, 1-mm isotropic resolution, time repetition [TR] = 18 ms, time echo [TE] = 10 ms, flip angle = 30°), T_2-weighted (2D multislice fast spin echo scan with 140–160 2-mm slices with a 1 mm overlap, TR = 3300 ms, TE = 35 ms), and proton density (as for T_2 scan but with TE = 120 ms) images of the whole head. Only T_1 image of each subject was applied in this study.

Measurements of Cortical Thickness

The native MR images were first registered into stereotaxic space (Talairach and Tournoux 1988) using a 9-parameter linear transformation (Collins et al. 1994). Simultaneously, images were corrected for nonuniformity artifacts using the N3 algorithms (Sled et al. 1998). The registered and corrected images were further segmented into gray matter, white matter, cerebrospinal fluid, and background using an advanced neural net classifier (Zijdenbos et al. 2002). The inner and outer gray matter surfaces were then automatically extracted from each MR volume using the Constrained Laplacian-based Automated Segmentation with Proximities (CLASP) algorithm (MacDonald et al. 2000; Kim et al. 2005) and cortical thickness was measured in native space using the linked distance between 2 surfaces at 40 962 vertices throughout the cortex. The measurement in native space provided an unadjusted estimate of absolute cortical thickness (Shaw et al. 2006). A representative cortical thickness map was shown in Figure 1*A*. The CLASP cortical thickness algorithm has been validated using both manual measurements (Kabani et al. 2001) and simulation approaches (Lerch and Evans 2005; Lee et al. 2006), and recently applied to Alzheimer's disease (Lerch et al. 2005) and cortical development studies (Shaw et al. 2006). Individual cortical thickness maps were parcellated using the Automated Nonlinear Image Matching and Anatomical Labeling package (Collins et al. 1995; Robbins et al. 2004). By registering each subject's MR images to a presegmented volumetric template using nonlinear deformations (Collins et al. 1995), the labels of brain regions were transformed to the cortical surface by assigning the value of the voxel label to each vertex on the surface. An average cortical parcellation was generated by finding the anatomical label with the highest occurrence at each vertex (Fig. 1*B*) and 27 separate cortical regions were identified for each hemisphere (Supplementary Table). Cortical thickness for each region was measured as the mean thickness of all vertices defined as belonging to that region.

Construction of Anatomical Connection Matrix

A key issue in characterizing human brain networks is the construction of the anatomical connection matrix (Sporns et al. 2005). To address this issue, in this study, we first defined anatomical connection as statistical associations in cortical thickness between brain regions (Fig. 1*C*). Such a morphometry-based connection concept has been introduced by the 2 recent studies (Worsley et al. 2005; Lerch et al. 2006). The statistical similarity in cortical thickness between 2 regions was measured by computing the Pearson correlation coefficient across subjects and interregional correlation matrix ($N \times N$, where N is the number of brain regions, here $N = 54$) of such connections was acquired using the 124 brains included in this study (Fig. 1*D*). Prior to the correlation analysis, a linear regression was performed at every region to remove the effects of age, gender, age–gender interaction, and mean overall cortical thickness; the residuals of this regression were then substituted for the raw cortical thickness values. Because the correlation analysis was performed for all $54 \times 53/2 = 1431$ pairs of regions, it was necessary to perform a multiple comparisons correction to test the significance of these correlations. We applied the false discovery rate (FDR) procedure (Genovese et al. 2002) to correct the multiple comparisons at a q value of 0.05. Using this threshold, we constructed a symmetric connection matrix (Fig. 1*E*), whose element was 1 if the cortical thickness correlation between 2 regions was statistically significant and 0 otherwise. This binarized connection matrix captures the underlying anatomical connection patterns of the human brain common to the population sample under study. The anatomical and statistical properties of this network are further characterized below. It is also possible to characterize the network with continuous weighting between nodes (Barrat et al. 2004; Jiang et al. 2004) but this leads to complications of statistical features descriptions in subsequent graph theoretical analysis. This initial study therefore confined itself to a simpler on–off connectivity analysis.

Anatomical Connections and Anatomical Distance

The binarized anatomical connection matrix can be visualized in 3D anatomical space (Fig. 1*F*) by locating cortical regions according to their y and z centroid stereotaxic coordinates. In this study, we also examined the relationship between the anatomical connections and their corresponding anatomical distance (Fig. 2). The anatomical distance between 2 regions was defined as Euclidean distance D_{ij} (in mm) between regional centroids: $D_{ij} = \sqrt{(x_i - x_j)^2 + (y_i - y_j)^2 + (z_i - z_j)^2}$ where (x_i, y_i, z_i) and (x_j, y_j, z_j) are the stereotaxic coordinates of the centroids for regions i and j. The connections with $D > 75$ mm were considered long-range connections shown in Figure 3. The Euclidean distance used in the present study provides an approximate reflection on the true physical distance (axonal length) of connections between regions and has been applied in previous functional brain networks studies (Salvador, Suckling, Coleman, et al. 2005; Salvador, Suckling, Schwarzbauer, et al. 2005; Achard et al. 2006).

Graph Theoretical Analysis

To perform a graph theoretical analysis, the anatomical connection matrix obtained above was described as an undirected graph G with N

nodes and K edges, where nodes represent brain regions and edges represent undirected connections between regions. In this study, we estimated 3 important metrics of the graph G, namely, the mean degree $\langle k \rangle$, the clustering coefficient C_p, and the characteristic path length L_p. The mean degree $\langle k \rangle$ of the graph G is the average of the degree over all nodes, where the degree k_i of a node i corresponds to the number of connections to that node. The clustering coefficient C_p of the graph G is the average of the clustering coefficient over all nodes, where the clustering coefficient C_i of a node i is defined as the number of existing connections between the node's neighbors divided by all their possible connections (Watts and Strogatz 1998). C_p is a measure of the extent of local cluster or cliquishness of the network. Clearly, $0 \leqslant C_p \leqslant 1$; and $C_p = 1$ if and only if the network is fully connected, that is, each node is connected to all other nodes. The characteristic path length L_p of the graph G is the smallest number of connections required to connect one node to another, averaged overall all pairs of nodes. L_p is a measure of the extent of average connectivity or overall routing efficiency of the network. In this study, we also defined the mean shortest path length L_i of a node i as the average of the shortest path lengths between this node and all other nodes in this network. The nodes with the smallest L_i or largest k_i were considered the hubs of the network (Achard et al. 2006).

To examine the small-world properties, the values of C_p^{real} and L_p^{real} of the anatomical network were compared with those of 1000 random networks. We generated these random graphs using the random rewiring procedure described by Maslov and Sneppen (2002) and Milo et al. (2002), which preserves the same number of nodes, mean degree $\langle k \rangle$, and degree distribution as the real network. Typically, a small-world network should fulfill the following conditions: $\gamma = C_p^{\text{real}}/C_p^{\text{rand}} > 1$ and $\lambda = L_p^{\text{real}}/L_p^{\text{rand}} \sim 1$ (Watts and Strogatz 1998). These 2 conditions can also be summarized into a simple quantitative measurement, small worldness, $\sigma = \gamma/\lambda > 1$ (Humphries et al. 2005; Achard et al. 2006), implying that the magnitude ratio between C_p^{real} and C_p^{rand} is greater than the magnitude ratio between L_p^{real} and L_p^{rand}. In this study, we primarily report the results of C_p^{real} and L_p^{real} of the anatomical network of the human brain based on the FDR thresholded correlation matrix (Genovese et al. 2002). It is reasonable that the small-world attributes can change with the correlation thresholds. When the threshold is increased, some weaker connections will be dropped out and the resulting graphs will become sparser, leading to a decrease of the mean degree (Fig. 4*A*). When the correlation threshold reaches an value of $R_{\max}$, the mean degree of the resulting network will be less than the log of the number of nodes [i.e., $\langle k \rangle < \log(N) = 3.99$] and small-world properties are not estimable (Watts and Strogatz 1998; Achard et al. 2006). To explore the influence of thresholding on the small-world attributes, in this study, we applied the maximum range of correlation thresholds ($0 < R < R_{\max}$, with an incremental interval of 0.01) to the correlation matrix, and repeated the small-world analysis for every R value.

In addition to the small-word attributes, we also examined the connectivity degree distribution of the brain network (Fig. 5). It has been demonstrated that the small-world networks can be classified into different categories (e.g., scale-free and exponentially truncated power-law distribution) according to their connectivity distributions and each of which exhibits specific network behaviors such as the resilience to random errors or hubs attacks (Albert et al. 2000; Amaral et al. 2000; Achard et al. 2006). Finally, the hub regions in this network were identified by using a regionally shortest path length L_i averaged over both hemispheres. To visualize the hubs, we also mapped the human brain network with the Pajek software package (http://vlado.fmf.uni-lj.si/pub/networks/pajek/) (Batagelj and Mrvar 1998) using a Kamada–Kawai layout algorithm (Kamada and Kawai 1989) (Fig. 6). To assess the importance of the hubs for the brain network, we individually eliminated the hub and nonhub regions from the network and compared the changes in the global properties (largest component size, clustering coefficients and characteristic path lengths) of the resulting networks using a 2-sample t test.

Results

Under the statistical threshold of p value of 0.05 (corrected by FDR), we observed that the 104 pairs of regions exhibited significant anatomical connectivity (cortical thickness correlations), which resulted in a binarized anatomical connection matrix with a sparsity of ~7.3% (104/1431). Furthermore, we observed a single component with 45 connected nodes and 9 disconnected nodes in the sparse matrix (Fig. 1*E*). In this study, the properties of a network were calculated on its largest component.

Interregional Anatomical Connections

About half of the connections (46/104; 44.2%) were intrahemispheric, involving brain regions in the same lobe and anatomically adjacent regions across different lobes. Several symmetrically interhemispheric connections (18/104; 17.3%) among certain bilaterally homologous regions in the cerebral hemispheres were also found to be very significant. In addition, we also observed significant asymmetrically interhemispheric connections between the nonhomologous regions in different hemispheres (40/104; 38.5%). Table 1 included the most significant 15 interregional cortical thickness connections (corrected $P < 1.0 \times 10^{-05}$) and their approximately associated white matter fibers measured by diffusion imaging in human.

Anatomical Connections and Anatomical Distance

Figure 2 demonstrated the dependencies of anatomical connectivity on anatomical distances. Most of the significant connections appeared to have shorter anatomical distances ($D < 75$ mm) but we also observed some long-range ($D > 75$ mm) connections in this brain network. The probability of finding a significant connection between any 2 regions for a given anatomical distance can be modeled as an exponentially truncated power law: $P(D) \sim D^{\alpha-1} e^{-D/D_c}$ with an estimated exponent $\alpha = 1.33$ and a cutoff distance $D_c = 35.2$ mm (Fig. 2*C*). This model indicates a scaling regimen, followed by an exponential decay in the probability of connections with an anatomical distance greater than a cutoff value of ~35 mm.

To further explore the pairs of regions that pertain to either the short- or the long-range connections, we visualized the connection map in the anatomical space (Fig. 3). In Figure 3*B*, we observed that short-range ($D < 75$ mm) connections (69; 66.3%) existed predominantly in the posterior cortex. Figure 3*C* indicated that long-range ($D > 75$ mm) connections (35; 33.7%) are mainly between regions of the frontal cortex (superior frontal gyrus [SFG], middle frontal gyrus [MFG], inferior frontal gyrus [IFG], medial front-orbital gyrus [MOFG] and precentral gyrus [PrCG]) and regions of the temporal (superior temporal gyrus [STG], middle temporal gyrus [MTG], inferior temporal gyrus [ITG] and lateral occipitotemporal gyrus [LOTG]), parietal (superior parietal lobe [SPL], precuneus [PCU], supramarginal gyrus [SMG] and angular gyrus [AG]) and occipital association cortices (superior occipital gyrus [SOG]).

Small-World Properties

In the present study, we calculated the clustering coefficient and characteristic path length for both of the cortical thickness connectivity network ($C_p^{\text{real}} = 0.30$, $L_p^{\text{real}} = 3.05$) and the corresponding random networks with the same number of nodes, mean degree, and degree distribution ($C_p^{\text{random}} = 0.13$, $L_p^{\text{random}} = 2.65$). In other words, the clustering coefficient of the brain network is approximately twice that of a comparable random network ($\gamma = 2.36$), whereas the path length is approximately equivalent to the random network ($\lambda = 1.15$),

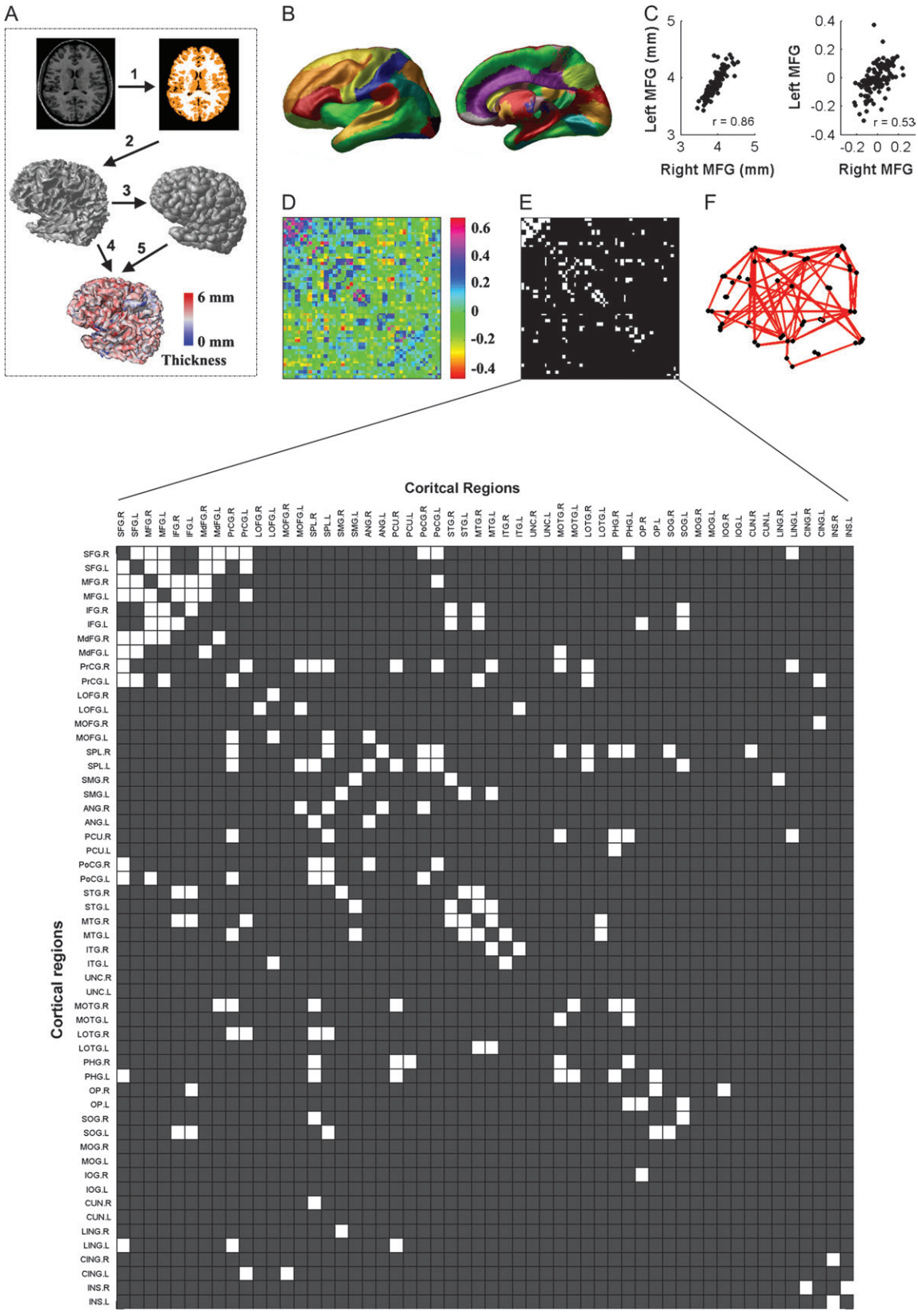

Figure 1. A flowchart for the construction of the human brain anatomical network using cortical thickness measurements from MRI. (*A*) Cortical thickness was estimated using computational neuroanatomy. The native images were nonuniformity corrected and registered into stereotaxic space. The resulting images were then classified (1) to extract the inner (2) and outer (3) gray matter surfaces. Cortical thickness was measured at each vertex (4,5). (*B*) The cerebral cortex was segmented into 54 cortical areas displayed on the average cortex, each color representing a different region. (*C*) Anatomical connection was defined as statistically association in cortical thickness between 2 areas. As an example of anatomical connections using cortical thickness correlations used in this study, we demonstrated that the thickness of right middle prefrontal gyrus had significant association with that of left middle prefrontal gyrus. The left plot showed the associations ($r = 0.86$, $P = 6.17 \times 10^{-37}$) using raw cortical thickness values but the right plot showed

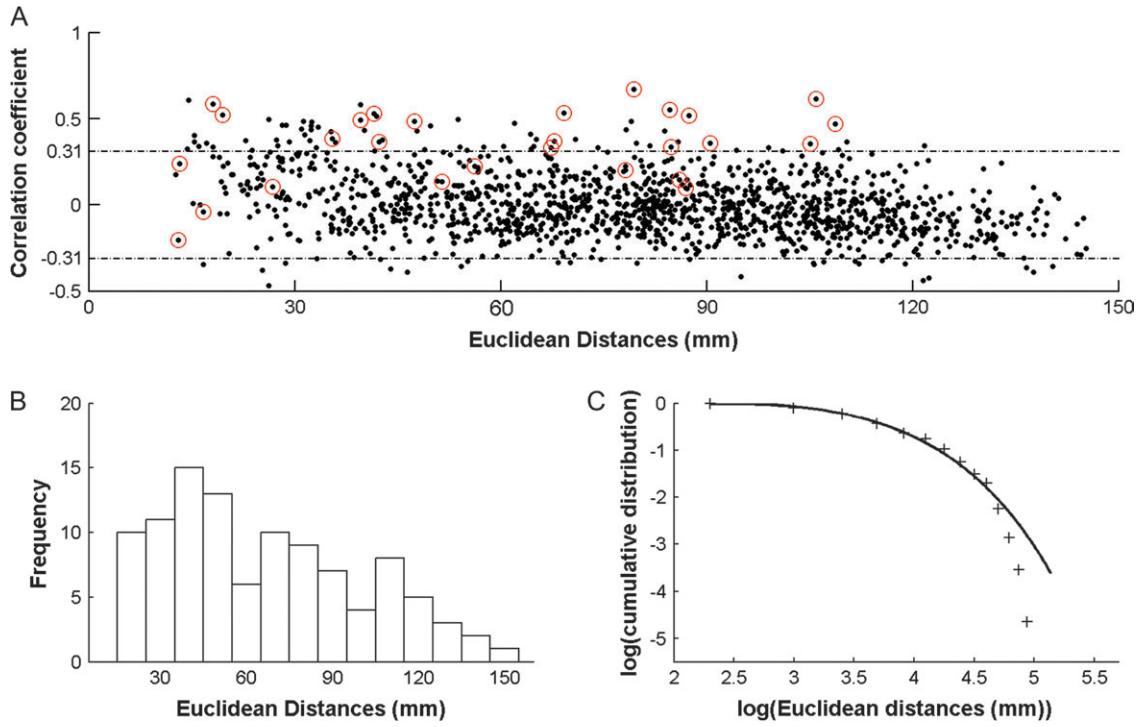

Figure 2. The dependencies of anatomical connectivity on anatomical distance. (*A*) Plot of anatomical connections (cortical thickness correlations) versus anatomical distance between regions. Red circles indicate the anatomical connections between bilaterally homologous regions. The dotted lines indicate the values of correlations under the FDR threshold ($P = 0.05$). (*B*) Distribution of anatomical distance. Frequency indicates the number of significant connections for a given anatomical distance. The figure shows many strong local-range connections and a few long-range connections. (*C*) Probability of finding a significant connection for a given distance in the log–log plot fitted by an exponentially truncated power law (black solid line). The observed data points (plus sign) were obtained by a FDR threshold. Distance shown in figures indicates Euclidean distance between regional centroids in stereotaxic space.

thus resulting in a small-world scalar parameter of $\sigma = 2.04$ (Table 2). In Figure 4, we showed the small-world properties of the anatomical network as a function of correlation threshold. For a lower threshold value, the corresponding brain network is almost fully connected and the small-world properties are indiscernible (both C_p^{real} and L_p^{real} are close to 1) from the matched random networks. As the correlation threshold values increased the clustering coefficient also increased rapidly (Fig. 4*D*), whereas the path length only changed slightly (Fig. 4*E*), leading to the increases of the small worldness (Fig. 4*F*). Overall, small-world properties were salient at higher threshold (Fig. 2*D–F*). The small-world models shown here therefore indicated that anatomical networks of the human brain have greater local interconnectivity or cliquishness and short mean distance between regions.

Connectivity Degree Distribution and Hub Regions

In addition to the investigation of the small-world properties, we also examined the degree distribution of the anatomical network in the human brain. Clearly, the brain network does not follow a power-law form because the fitted curve is not a straight line on the log–log plot (Fig. 5). Rather, this distribution can be well fitted by an exponentially truncated power-law form: $P(k) \sim k^{\alpha-1} e^{-k/k_c}$ with an estimated exponent $\alpha = 1.38$ and a cutoff degree $k_c = 2.50$. This model indicates a scaling regimen, followed by an exponential decay in the probability of finding nodes with a connection degree greater than a cutoff value of ~3. In addition, we also demonstrated that the exponentially truncated power-law distribution was apparent under several different correlation thresholds with only a slight change in the values of estimated parameters (Fig. 5). This distribution model indicated that the brain networks included some hub nodes with many connections but prevented the appearance of huge hubs with very many connections.

Twelve hub nodes of this network were identified by using a regionally shortest path length averaged over both hemispheres. These hubs included 9 regions of the heteromodal or unimodal association cortex, 2 regions of the primary motor and sensorymotor cortex and one region of the paralimbic cortex (Fig. 6, Table 3), which had a large overlap with the hub nodes identified in a very recent functional brain network study

associations ($r = 0.53$, $P = 1.76 \times 10^{-10}$) using the residuals of cortical thickness obtained by removing the effects of gender, age, gender–age interaction, and mean overall cortical thickness. It was noted that the use of the residuals removed some of correlations between regions. Each data point represents a single subject in the study. (*D*) Correlation matrix of the cortical thickness in the human brain was acquired using the 124 brains from the ICBM database. (*E*) Anatomical connection matrix was constructed by thresholding the correlation matrix in (*D*) using a FDR procedure. The labeled matrix was presented below. Note that the matrix shown here only included interregional pathways with strong correlations due to the conservative FDR threshold (Genovese et al. 2002) used to in this study. The sparse matrix was composed of 45 connected nodes and 9 disconnected nodes including several unimodal (bilateral cuneus, bilateral middle occipital gyrus, and left inferior occipital gyrus), paralimbic, and limbic regions (bilateral uncus, bilateral insula, and right cingulate region). R, right; L, left. For the abbreviations of the regions, see Supplementary Table. (*F*) The thresholded connection matrix was visualized in anatomical space. For details, see Materials and Methods.

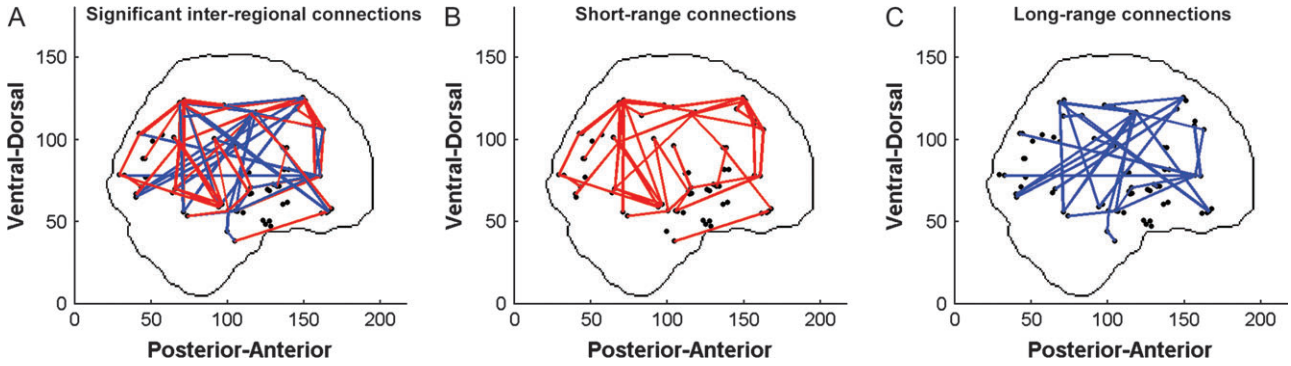

Figure 3. Short- and long-range anatomical connections in the anatomical space. (*A*) One hundred and four undirected edges (~7.3% of the 1431 possible connections among regions) representing the significant connections were shown in a sagittal view of the brain. Edges were classified into (*B*) short-range connections ($D < 75$ mm, red) and (*C*) long-range connections ($D > 75$ mm, blue) The locations of the nodes indicated the *y* and *z* coordinates of the regional centroids in Talairach space.

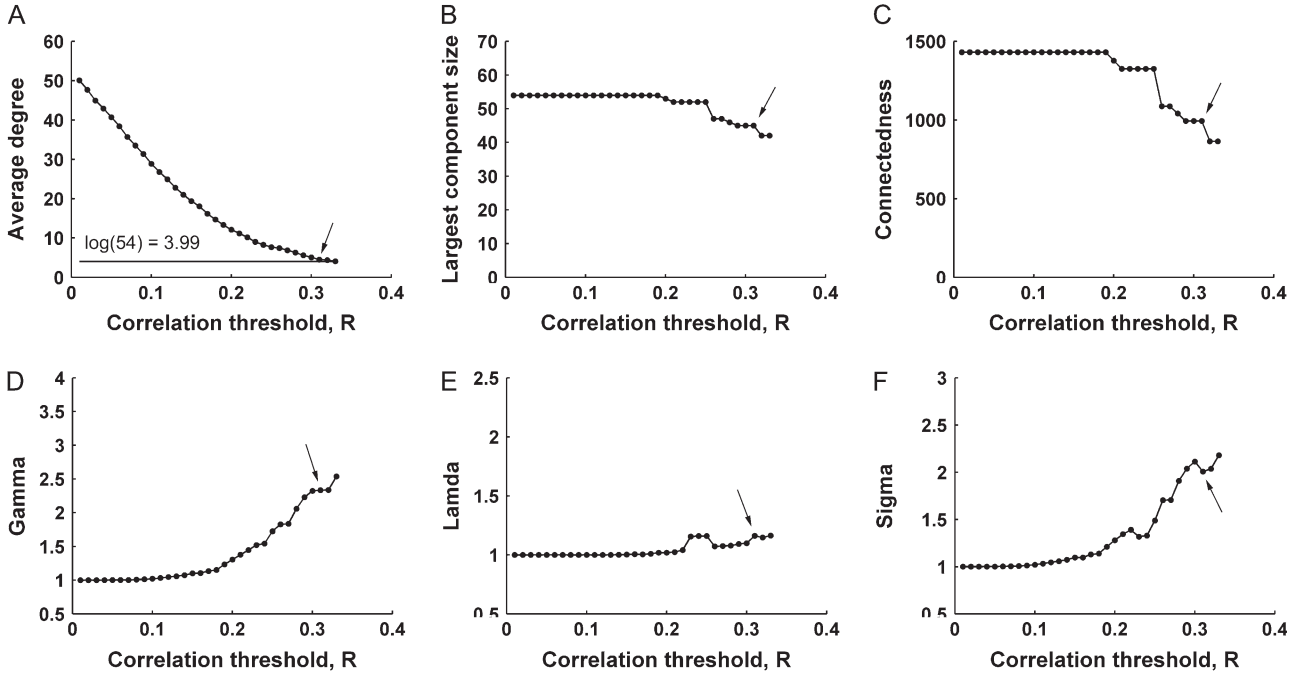

Figure 4. Small-world properties of the anatomical networks as a function of correlation threshold. (*A*) The mean degree of human brain anatomical networks decreases as the correlation threshold increases. Small-world properties are not estimable when the mean degree of anatomical network obtained under the correlation threshold R_{max} is less than $\log(N) = 3.99$ (Watts and Strogatz 1998; Achard et al. 2006). (*B*) The largest component size decreases as the correlation threshold increases. (*C*) The connectedness tends to decrease as the correlation threshold, where the connectedness is assessed by the reachability matrix recording if at least one path exists between all pairs of nodes (Sporns et al. 2000). (*D*) The clustering coefficient increases as the correlation threshold increases. (*E*) The path length has relatively small changes as the correlation threshold increases. (*F*) The small worldness tends to increase as the correlation threshold increases. The black arrows indicate the values of small-world properties of the human brain anatomical network constructed by a FDR threshold.

(Achard et al. 2006). To elucidate the importance of these hub regions for the brain network, we removed the hub and nonhub regions separately and compared the global properties of the resulting 2-group networks (Fig. 7). Compared with the nonhubs, the elimination of the hub regions only resulted in slight changes in the largest component size ($t = 0.31$, $P = 0.76$) but significant decreases in the clustering coefficient ($t = -4.80$, $P = 8.67 \times 10^{-5}$) and increases in the characteristic path length ($t = 4.91$, $P = 6.50 \times 10^{-5}$). In addition, we also found that, when individual hub node was removed from the brain network, the characteristic path lengths of the resulting networks were larger than those ($L_p^{real} = 3.05$) of the experimental network (Table 3).

Discussion

This is the first study, to our knowledge, to demonstrate the large-scale anatomical connectivity patterns in the entire human cerebral cortex using cortical thickness measurements. We found significant short- and long-range anatomical connections (cortical thickness correlations) in both intrahemispheric and interhemispheric regions. More importantly, we showed that the human brain anatomical network had small-world properties with cohesive neighborhoods and short path length between regions. In addition, we also demonstrated that both the anatomical network and the probability of finding a connection between 2 regions for a given anatomical distance followed an exponentially truncated power-law model. Taken together,

we concluded that our results provided an important structural description for the network of anatomical connections in the human brain.

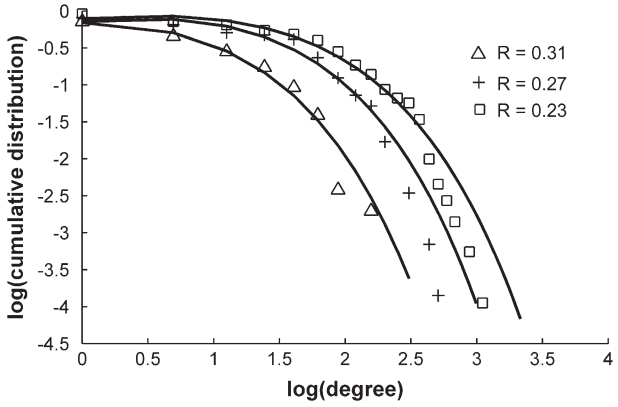

Figure 5. The degree distributions of human brain anatomical networks for 3 different correlation threshold values. The black solid lines indicate exponentially truncated power-law fits in the log–log plot of the cumulative probability degree versus the degree for the 3 correlation threshold values. Here a cumulative distribution was used to reduce the effects of noise on this smaller data set (Strogatz 2001). Upright triangles: correlation threshold $R = 0.31$ (corresponding to P value of 0.05 corrected by FDR); mean degree $\langle k \rangle = 5.4$; estimated exponent $\alpha = 1.38$; and cutoff degree $k_c = 2.50$. Plus sign: correlation threshold $R = 0.27$; mean degree $\langle k \rangle = 7.0$; estimated exponent $\alpha = 1.13$; and cutoff degree $k_c = 1.43$. Squares: correlation threshold $R = 0.23$; mean degree $\langle k \rangle = 9.0$; estimated exponent $\alpha = 1.09$; and cutoff degree $k_c = 1.32$.

Interpreting Cortical Thickness Correlations

Human neuroanatomy is less well developed than nonhuman neuroanatomy because the common invasive tracer methods cannot be applied to the human brain (Crick and Jones 1993). Thus, the patterns of anatomical connections in the human brain remain unclear. Recent noninvasive diffusion MRI techniques have provided a promising experimental route toward revealing the connectivity patterns in vivo in human but there continues to be some limitations in data acquisition and processing approaches such as the issues of crossing or intersecting fibers (Dougherty et al. 2005; Tuch et al. 2005). Here we proposed a new avenue of research to explore the patterns of anatomical connectivity in the human brain. A prominent difference between the current analysis and previous studies on the human anatomical substrates is that, in the current study, 2 areas are considered anatomically connected if they show statistically significant associations in cortical thickness. Although the exact biological nature of the cortical thickness correlations is still unknown, it has been argued that the covariation of the morphological features (tissue volume or concentration) in related cortical regions may be resulted from the mutually trophic influences (Ferrer et al. 1995), the contribution of heredity (Suddath et al. 1990; Steinmetz et al. 1994; Thompson et al. 2001), or common experience-related plasticity (Maguire et al. 2000; Draganski et al. 2004; Mechelli et al. 2004). Recently, studies have also indicated that these intercorrelated regions may be a part of functional, neuroanatomically interconnected systems (Andrews et al. 1997; Wright et al. 1999; Mechelli et al. 2005; Mitelman et al. 2005). For instance, Andrews et al. (1997) observed that

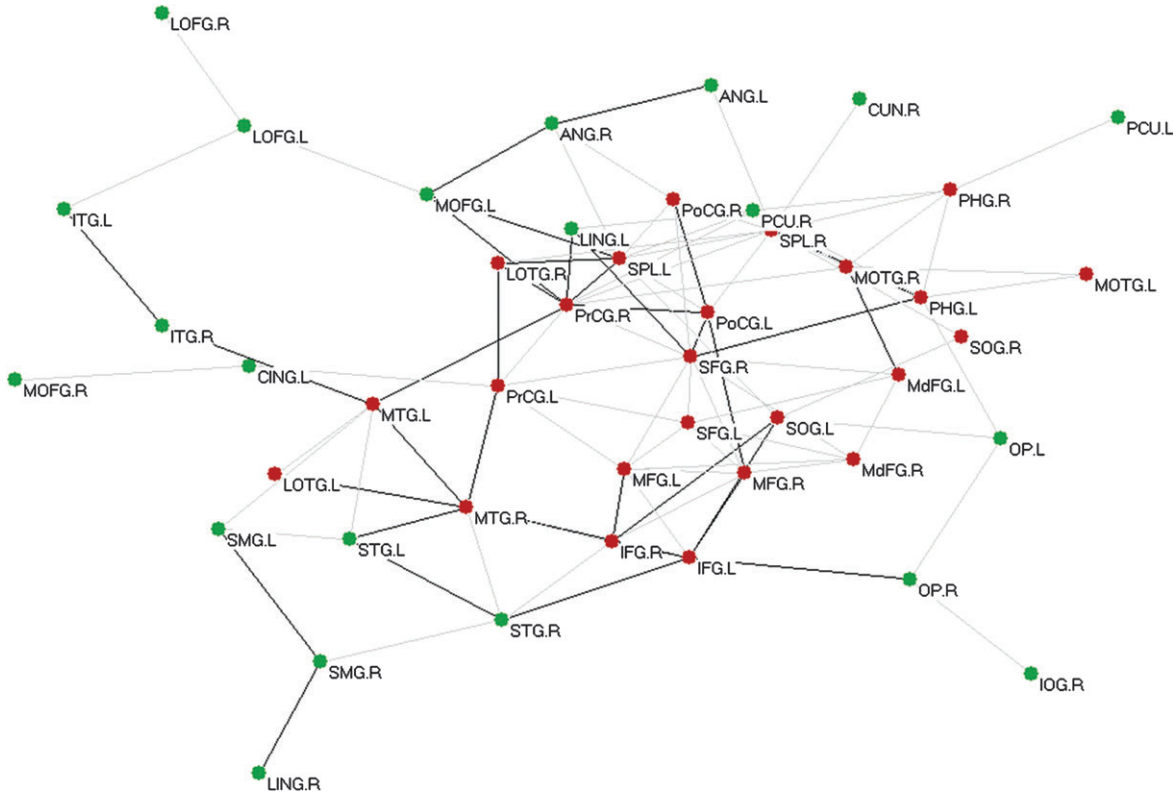

Figure 6. The topology of human brain anatomical network representing significant cortical thickness correlations. Regions are represented as nodes, and connections are represented as edges that link the nodes. Hubs regions are colored in red and nonhub regions are colored in green. Black lines represent long-range connections ($D > 75$ mm) and gray lines represent short-range connections. The geometric distance between regions on the drawing space approximates the shortest path length between them. The network was visualized with the Pajek program (Batagelj and Mrvar 1998). For the abbreviations of the regions, see Supplementary Table.

Table 1
The most significant 15 interregional cortical thickness correlations (corrected $P < 1.0 \times 10^{-05}$) and their approximate associated fiber tracts

No.	Region A	Region B	Class	Correlations		*D* (mm)	Approximate associated fiber tracts
				R	Corrected *P*		
1	PoCG.R	PoCG.L	SIH	0.67	1.96×10^{-13}	**79.4**	The midbody in the CC[a,b]
2	MTG.R	MTG.L	SIH	0.62	1.63×10^{-10}	**105.9**	The splenium in the CC[b]
3	SFG.R	MdFG.R	IH	0.61	2.73×10^{-10}	14.5	SLF[c,e]
4	MdFG.R	MdFG.L	SIH	0.58	2.78×10^{-09}	18.1	The genu and anterior part of the body in the CC[a,b]
5	SPL.L	PoCG.L	IH	0.58	2.78×10^{-09}	39.6	SLF[c,e]
6	PrCG.R	PrCG.L	SIH	0.55	6.47×10^{-08}	**84.6**	The midbody in the CC[a,b]
7	MFG.R	MFG.L	SIH	0.53	2.82×10^{-07}	69.2	The genu and anterior part of the body in the CC[a,b,d]
8	LOFG.R	LOFG.L	SIH	0.53	4.20×10^{-07}	41.6	The rostrum in the CC[d]
9	PHG.R	PHG.L	SIH	0.52	6.04×10^{-07}	19.5	The splenium in the CC[b]
10	IFG.R	IFG.L	SIH	0.52	7.85×10^{-07}	**87.4**	The genu and anterior part of the body in the CC[a,b]
11	SFG.L	PrCG.L	IH	0.51	1.03×10^{-06}	41.9	SLF[c,e]
12	STG.R	MTG.R	IH	0.50	4.25×10^{-06}	26.2	U-fibers[c]
13	PrCG.R	SPL.R	IH	0.49	4.79×10^{-06}	53.8	SLF[c,e]
14	SFG.R	SFG.L	SIH	0.49	5.16×10^{-06}	39.6	The genu and anterior part of the body in the CC[a,b,d]
15	SFG.L	MFG.L	IH	0.49	7.25×10^{-06}	31.3	U-fibers[c]

Note: List of the 15 pairs of connected regions (descending order of statistical significance) with the most significant cortical thickness correlations (corrected by FDR). These connections were classified into intrahemispheric (IH, 6) and symmetrically interhemispheric (SIH, 9) connections. *R* and *P* denote the cortical thickness correlation coefficients between regions and their corresponding significant levels. *D* denotes the Euclidean distance, defined as the distance between each pair of regional centroids in stereotaxic space. A pair of regions with $D > 75$ mm was considered long-range connections in bold and short-range connections otherwise. Approximate associated fiber tracts for each cortical thickness correlation observed in this study were listed the rightmost column. Note that the cortical thickness correlations among regions were calculated after removing the effects of age, gender, age–gender interaction, and mean overall cortical thickness. See supplementary Table for the abbreviations of the regions.

[a]Hofer and Frahm 2006.

[b]Zarei et al. 2006.

[c]Wakana et al. 2004.

[d]Huang et al. 2005.

[e]Makris et al. 2005.

Table 2
Small-world properties of brain networks shown in the present study and previous studies

Brain networks	*N*	C_p	L_p	γ	λ	σ
Human: anatomical network (the present study)	54	0.30	3.05	2.36	1.15	2.04
Human: functional network (Achard et al. 2006)	90	0.53	2.49	2.37	1.09	2.18
Human: functional network (Salvador, Suckling, Coleman, et al. 2005)	45	0.25	2.82	2.08	1.09	1.91
Macaque: anatomical network (Sporns and Zwi 2004)	71	0.46	2.38	1.92	1.12	1.70
Cat: anatomical network (Sporns and Zwi 2004)	52	0.55	1.81	1.37	1.05	1.30

Note: *N*, C_p, and L_p denote the number of nodes, clustering coefficient, and mean shortest path length of the real brain networks, respectively. γ denotes the ratio of the clustering coefficient between the brain networks and the constructed random networks. λ denotes the ratio of the mean shortest path length between the brain networks and the constructed random networks. In the present study, these random graphs were generated using a random rewiring procedure (Maslov and Sneppen 2002). σ is a ratio of γ and λ, measuring the small worldness of a network. For the details, see Methods and Materials. Note that the small-world attributes shown in the present investigation are much closer to those of the human brain functional networks, compared with those of the anatomical brain networks of macaque and cat.

several components of the human visual system (i.e., the optic tract, lateral geniculate nucleus, and primary visual cortex) covary in volume across individuals. Significant regional gray matter volumetric or concentration correlations were also found in the frontal-temporal (Woodruff et al. 1997; Bullmore et al. 1998; Mitelman et al. 2005) and frontal-parietal systems (Wright et al. 1999; Mechelli et al. 2005). One vital support for the present study is that Lerch et al. (2006) demonstrated a striking similarity between the cortical thickness correlation maps of Brodmann Area 44 and diffusion tensor maps of the arcuate fasciculus (a language-related neural pathway connecting Broca's and Wernicke's areas), suggesting that they were measuring 2 aspects of the same underlying processes. All these processes are the likely driving forces behind the patterns of anatomical connections of the human brain herein.

Cortical Thickness Correlations and Neuroanatomical Pathway

In this study, we detected 104 pairs of regions showing significant correlations in cortical thickness. A question of interest is whether the regions found to be associated in the present investigation are also related to the neuroanatomical pathway of the human brain. To address this issue, we matched the 15 most significant (corrected $P < 1.0 \times 10^{-05}$) connections to the approximate associated anatomical connections obtained from previous human diffusion imaging studies (Table 1). Several significant correlations were present in homologous regions in a bilateral and symmetrical fashion; this finding can be explained by the associations between these regions through the corpus callosum (CC), a crucial white matter structure providing interhemispheric communications between both hemispheres of the brain. Indeed, it has been suggested that the parcellation of the CC in vivo into several major subdivisions such as the genu, the body, and the splenium, is based on the transit of interhemispheric pathways connecting homologous brain areas (Huang et al. 2005; Hofer and Frahm 2006; Zarei et al. 2006). Thus, tracts connecting to prefrontal cortex occupy the genu and anterior part of the body of the CC. Moreover, connections of the central brain regions such as the primary motor and sensorymotor cortex are located within the midbody

Table 3
Regions of the human brain anatomical network and their statistical properties

Regions	Class	L_i	k_i	C_i	N'	C'_p	L'_p
PrCG	Primary	2.19	9.00	0.25	43.00	0.30	3.17
SFG	Association	2.50	8.50	0.47	44.00	0.29	3.10
SPL	Association	2.32	10.00	0.26	43.50	0.29	3.13
MTG	Association	2.51	6.50	0.25	44.00	0.27	3.22
PoCG	Primary	2.53	4.50	0.60	44.00	0.29	3.08
MFG	Association	2.59	7.00	0.50	44.00	0.30	3.08
IFG	Association	2.62	5.50	0.33	44.00	0.30	3.18
PHG	Paralimbic	2.76	6.00	0.40	43.50	0.29	3.07
SOG	Association	2.79	4.00	0.05	44.00	0.31	3.10
LOTG	Association	2.80	3.00	0.84	44.00	0.29	3.06
MOTG	Association	2.86	4.50	0.69	44.00	0.29	3.07
MdFG	Association	2.92	4.50	0.65	44.00	0.30	3.05
STG	Association	3.06	4.50	0.45	44.00	0.30	3.07
OP	Primary	3.06	2.50	0.00	43.50	0.32	3.02
ANG	Association	3.08	3.00	0.17	44.00	0.31	3.05
PCU	Association	3.21	3.50	0.20	44.00	0.31	3.04
CING	Paralimbic	3.22	2.00	0.00	43.00	0.32	2.98
CUN	Association	3.29	1.00	0.00	44.00	0.31	3.04
MOFG	Paralimbic	3.41	3.50	0.24	44.00	0.30	3.03
SMG	Association	3.45	2.50	0.00	43.50	0.32	3.00
ITG	Association	3.60	2.50	0.17	44.00	0.31	3.04
LING	Association	3.63	3.00	0.25	44.00	0.30	3.02
LOFG	Paralimbic	3.95	2.00	0.00	43.50	0.32	2.97
IOG.R	Association	4.11	1.00	0.00	44.00	0.31	3.00

Note: The hub regions (in bold) in the anatomical network of the human brain were identified using a regionally shortest path length L_i and they were listed in an ascending order of L_i. These regions were classified as Primary, Associations, and Paralimbic as described by Achard et al. (2006). k_i and C_i denote the degree and clustering coefficient of each region. N', C'_p, and L'_p denote the largest component size, clustering coefficient, and characteristic path length of the resulting network when region i was individually eliminated from the brain network. Note that when the hub nodes were removed from the brain network, the path length L'_p of the resulting network is larger than the path length L_p^{real} (3.05) of the experimental network. For the abbreviations of the regions, see Supplementary Table.

of the CC; the interhemispheric connections of the parietal cortex are located within the posterior part of the body and splenium. Finally, connections of the temporal and occipital cortex transit most exclusively through the splenium of the CC. These results from diffusion imaging studies provide an important support for our findings of symmetrically interhemispheric correlations in cortical thickness. In addition to the interhemispheric connections, we also observed significant intrahemispheric connections between SFG–MdFG, SFG–PrCG, SPL–PrCG and SPL–PoCG (Table 1) that are all associated with the superior longitudinal fascicle (SLF) linking the caudodorsal prefrontal cortex with the premotor (PrCG), supplementary motor (MdFG), and superior parietal regions (SPL) (Wakana et al. 2004; Makris et al. 2005). All those areas and the network they form via the SLF are involved in the control of reaching and, more generally, movement in space (Mountcastle et al. 1975; Lacquaniti et al. 1995). The connections between adjacent areas STG–MTG and SFG–MFG (Table 1) are examples of short association fibers (e.g., U-fibers) that provide the means of interaction for those adjacent areas participating in common computations: language processing (STG–MTG) and higher-order cognitive control (SFG–MFG) (Wakana et al. 2004; Petrides 2005). Additionally, in this study, we also observed significant cortical thickness correlations among the IFG, STG, and SMG regions (Fig. 6), which were consistent with previous cortical thickness correlation study (Lerch et al. 2006) and fiber tracking (arcuate fasciculus) study (Parker et al. 2005). Taken together, these significant cortical thickness correlations observed in the present study are related to the major fibers tracts (CC and SLF) or short association fibers (U-fibers). One could therefore speculate that the morphometry-based corticocortical correlates provide approximate reflection on the true anatomical connections among neuronal elements. A detailed investigation on the cortical thickness correlations and their

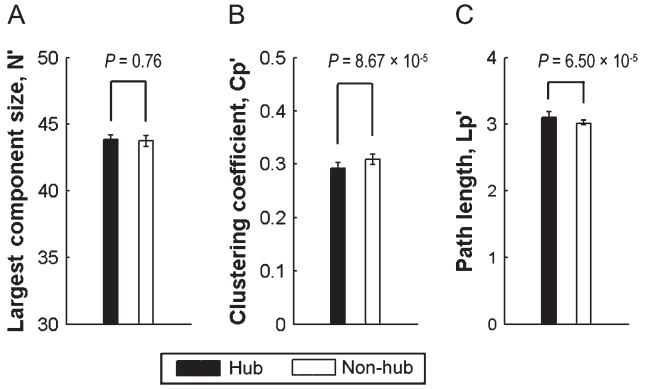

Figure 7. The comparison of the impacts of hub and nonhub regions on network properties. (*A*) The elimination of the hubs did not significantly affect the largest component size but (*B*) significantly decreased the clustering coefficient and (*C*) increased the path length of the resulting network in comparison with the elimination of the nonhub nodes. For the details of the hubs in the brain network and their statistical properties, see Table 3.

corresponding anatomical connections in the human brain will be an important topic for future studies.

In this study, we also observed differences in connectivity patterns in the left and right hemispheric regions, such as the medial and lateral orbital frontal gyrus, AG, and lingual gyrus (Fig. 6). Previous studies have reported structural and functional asymmetries in several regions of human cortex, including frontal, temporal, and occipital regions (for a review, see Toga and Thompson 2003). Furthermore, Mechelli et al. (2005) have also demonstrated interregional asymmetric patterns of associations in gray matter concentration, providing further support for our finding of connection patterns differences in 2 hemispheric regions. In future, it would be interesting to examine the asymmetric cortical thickness associations in details using

the "seed" regions of interest methods described by Mechelli et al. (2005).

Anatomical Connections and Anatomical Distance

Using cortical thickness measurements, in the present study, we found many short-range connections as well as some long-range connections (Figs. 2 and 3). Several recent functional connectivity studies using fMRI have also demonstrated the local and long-range connections in the human brain (Salvador, Suckling, Coleman, et al. 2005; Salvador, Suckling, Schwarzbauer, et al. 2005; Achard et al. 2006) that are consistent with our results. As noted in previous section, short-range/local connections may be associated with the short fibers (arcuate or U-fibers) that constitute the local circuitry but long-range connections may be associated with the commissural fibers (right–left hemispheric connections) and intrahemispheric association fibers (e.g., SLF) (Wakana et al. 2004). In this study, we also demonstrated the dependencies of anatomical connectivity on anatomical distance, characterized as a power-law form with an exponential cutoff, implying that the probability of finding a connection is distributed by a scale regimen, followed by an exponential decay in probability of connections with an anatomical distance greater than a cutoff value (~35 mm). Such spatial constraints on connections are biologically realistic and have been acknowledged in many biological systems. It has been suggested that the likelihood of long-range connections among macaque cortical regions decreases with distance, partly because the concentration of diffusible signaling and growth factors decays with distance (Sporns et al. 2004). Recently, the computational models of cortical development based on this physical principle have been proposed to understand the relationship of cortical morphology and the connectivity of normal brains (Hilgetag and Barbas 2006). These investigations provide important support for our findings of the dependencies of anatomical connectivity on anatomical distance in the human brain. It is also noted that, although the number of long-range connections is limited in the brain networks, they might constitute shortcuts to ensure short mean path lengths of the whole networks (Kaiser and Hilgetag 2004).

Small-World Anatomical Networks of the Human Brain

The coexistence of many short-range anatomical connections as well as some long-range connections raised the possibility that the anatomical network of the human brain might have small-world properties. Because it was introduced by Watts and Strogatz (1998), the small-world model has made a tremendous impact on the studies of numerous complex networks, from social, economic to biological networks (for a review, see Strogatz 2001). The model characterizes the architecture of the networks with well-connected local neighborhoods and short mean distance between nodes. Recent studies have suggested that the human brain functional networks constructed from fMRI (Eguiluz et al. 2005; Salvador, Suckling, Coleman, et al. 2005; Achard et al. 2006), EEG (Micheloyannis et al. 2006; Stam et al. 2007) and MEG (Stam 2004) data along with nonhuman cortical networks derived from anatomical tract-tracing method (Hilgetag et al. 2000; Stephan et al. 2000; Sporns and Zwi 2004) have small-world properties. Our results demonstrate for the first time that such properties are also the characteristics of large-scale anatomical networks of the human cerebral cortex (Fig. 4). The 2 main features for the small-world topology, high clustering coefficient and short path length, indicate the local clustering or cliquishness of the connectivity network and the small number of connections between any pair of regions. Previous optimal study using computational simulation (Sporns et al. 2000) has demonstrated the emergence of small-world topologies when networks are evolved for high complexity (defined as the coexpression of local specialization and global integration; Tononi et al. 1998; Sporns and Tononi 2002). Thus, our finding of small-world attributes in the cortical thickness networks reflects a near-optimal organizational pattern for the evolution of human brain structures. Furthermore, we proposed that the optimal design of the human brain anatomical network might have important implications for understanding how functional brain states emerge from their structural underpinnings. It has been suggested that the structure of the cerebral cortex is intimately associated with its function, as many other biological systems (Sporns and Zwi 2004). High clustering assures the modularized information processing, which are functionally segregated from one to another. Short paths assure effective interactions or rapid transfer of information between regions, which are essential for functional integration. The coexistence of functional segregation and functional integration guarantees the effective integration of multiple segregated sources of information (Tononi et al. 1994; Sporns and Zwi 2004; Sporns et al. 2004). Our results of small-world properties reported here might thus provide the underlying structural substrates of such functional coexistence in the human brain.

To further address the associations between structural and functional networks of the human brain, we compared our results with the values of small-world properties from previous brain network studies (Sporns and Zwi 2004; Salvador, Suckling, Coleman, et al. 2005; Achard et al. 2006) in Table 2. Our measurements of small-world properties in the human cortical anatomical network are $\gamma = 2.36$, $\lambda = 1.15$, and $\sigma = 2.04$. Salvador, Suckling, Coleman, et al. (2005) and Achard et al. (2006) reported the values in human brain functional networks: $\gamma = 2.08$, $\lambda = 1.09$, $\sigma = 1.91$, and $\gamma = 2.37$, $\lambda = 1.09$, $\sigma = 2.18$, respectively, whereas Sporns and Zwi (2004) reported the values in nonhuman cortical anatomical networks: $\gamma = 1.92$, $\lambda = 1.12$, and $\sigma = 1.70$ for macaque whole cortex and $\gamma = 1.37$, $\lambda = 1.05$, and $\sigma = 1.30$ for cat whole cortex (Table 2). As expected, the values of small worldness in this study are in closer proximate to those of the human brain functional networks than macaque and cat anatomical networks. Additionally, we also found our absolute values for C_p and L_p ($C_p^{\text{real}} = 0.30$ and $L_p^{\text{real}} = 3.05$) had a good match with Salvador, Suckling, Coleman, et al.'s (2005) study ($C_p^{\text{real}} = 0.25$and $L_p^{\text{real}} = 2.82$). However, it should be noted that the present study and previous functional imaging studies used different subject populations and image analysis methods, such as different regional parcellation schemes and correlation threshold selections. These factors might have an impact on the construction of the anatomical/functional connection matrix that could eventually influence the comparability of these results. Thus, these different groups' comparisons in the values of small-world properties should be made cautiously. A systematic exploration for the network properties of the human brain using anatomical and functional data obtained within the same subjects could offer a more practicable strategy for mapping the associations of structural and functional properties. Overall, combined the previous results and the current findings, we concluded that small-world

properties might be a general principle of structural and functional organization of complex brain networks.

The Human Brain Anatomical Network is not Scale Free

In addition to the small-world properties, another important finding of this study is that the large-scale anatomical network of the human brain has an exponentially truncated power-law degree distribution as opposed to a scale-free distribution (Fig. 5). This result is largely compatible with previous studies in human brain functional networks (Achard et al. 2006) and nonhuman cortical anatomical networks (Sporns and Zwi 2004). This truncated power-law distribution indicates that the human brain network has some "core" regions but prevents the appearance of the huge hubs with very many connections. Compared with a scale-free network, such a network structure shown here is more resilient to targeted attacks but equally resilient to random errors (Albert et al. 2000; Achard et al. 2006). Although the biological causes underlying this network topology remain unclear, physical constraints on the number of afferent connections a neuron can support render the exponentially truncated power-law possible mechanism in neuronal development (Sporns and Zwi 2004). Our results of the dependencies of interregional anatomical connections on the anatomical distance (Euclidean distance) (Fig. 2) provide further support for this view.

In the present study, we also identified several hub regions in the anatomical network of the human brain (Fig. 6, Table 3), most of which are the heteromodal or unimodal association cortex receiving convergent inputs from multiple cortical regions. Many hubs (e.g., SFG, SPL, MTG, MFG, IFG, and SOG) observed here are in accordance with the findings in the functional brain network by Achard et al. (2006). It has been argued that hubs in the brain networks are regions with multimodal or integrative function and their damages can remarkably affect the stability and efficiency of the network (Sporns and Zwi 2004; Achard et al. 2006). In the brain anatomical network, while comparing with the nonhub regions, the elimination of the hub regions leads to significant decreases of the clustering coefficients and increases of the path lengths (Fig. 7), though the largest component size of the resulting networks remains significantly unaffected, suggesting that the hubs might be of particular importance for not only the existence of highly local clustering but also the overall routing efficiency of the brain network (the small-world behavior). We therefore suspected that the patients (e.g., schizophrenia and Alzheimer's disease) with the known structural and functional abnormality of the association cortex might have altered small-world properties in the anatomical networks, which could be examined in the future investigations.

Methodological Issues

Some methodological issues of the present study need to be addressed. First, we used fully automatic and operator-independent procedures to measure the cortical thickness from MRI. The concern is that the cortical thickness measurement results could be potentially influenced by the scanning protocols (Han et al. 2006) and image processing methods implemented (Lerch and Evans 2005). Second, we applied a conservative FDR threshold (Genovese et al. 2002) to construct the anatomical connection matrix of the human brain, which allowed us to examine only those pathways with strong correlations. Currently, it is difficult to determine a definitive threshold in the construction of complex brain networks based upon correlation methods, such as the human brain functional network derived from fMRI (Salvador, Suckling, Coleman, et al. 2005; Achard et al. 2006) or EEG data (Micheloyannis et al. 2006; Stam et al. 2007). Future investigations in the continuous weighted brain networks could be helpful to avoid the thresholding issues. Here we found that our selected threshold caused a relatively low sparsity (~7.3%) in comparison with the sparsity of the anatomical connectivity matrices of macaque [~15%, 746/(71 × 70)] and cat [~33%, 820/(52 × 51)] (Sporns and Zwi 2004). However, it is difficult to compare the sparsity of this matrix with the anatomical matrices of macaque and cat because they were established using different methods: The anatomical matrices in macaque and cat were derived from tract-tracing data but our matrix was obtained from the thresholded cortical thickness correlations. Despite this, we still examined the properties of our cortical thickness network with a 15% sparsity, which corresponds to the 15% sparsity in the macaque anatomical network (Sporns and Zwi 2004) and found $\gamma = 1.7$ and $\lambda = 1.16$. Though at 31%, which corresponds to the 31% sparsity in the cat anatomical network (Sporns and Zwi 2004), our network had a reduced small-world properties, $\gamma = 1.14$ and $\lambda = 1.005$. The discrepancies could be due to the fact that there is a higher structural similarity in the cerebral cortex between the human and macaque than the human and cat. Third, a prior volumetric template was employed to automatically parcellate the entire cerebral cortex into different regions (Collins et al. 1995). Such an atlas-based parcellation allows us to characterize the large-scale connectivity pattern for the human brain networks; however, one of the problems is that there is interindividual variability in the anatomical boundaries of regions. Currently, there is no single acceptable strategy for the cortical parcellation, the validity of the parcellation thus mostly depends on the suitability of the applied atlas. Nonetheless, several recent studies have investigated the functional or anatomical connectivity pattern in the human brain using such an atlas-based parcellation strategy (Wright et al. 1999; Salvador, Suckling, Coleman, et al. 2005; Achard et al. 2006). In future studies, it might be more meaningful to parcellate the cerebral cortex based on a finer myeloarchitectonic feature. In addition, it is also helpful to explore the impact of different parcellation schemes on the network architectures. Fourth, we described a large-scale structural organization for human brain anatomical networks using the cortical thickness measurements. Currently, such a macroscale description is more practical to reveal the anatomical connectivity patterns of the human brain than microscale and mesoscale descriptions because of its relatively low computational load and simple definition in neuronal elements (regions) and connections. Further investigations could involve the characterization of connection patterns among neuronal elements such as cortical vertices and assess the dependencies of the network architectures on spatial scales. Finally, we used cortical thickness measurements as a morphological feature to construct the anatomical connection matrix of the human brain and further described its anatomical and statistical properties. The morphological features can also include surface area, tissue volume, tissue density, and others. Our recent study (in preparation) demonstrates that the gray matter volume networks in the human brain also have the small-world properties, which are consistent with the present study. It will be interesting to explore more detailed patterns using these morphological features.

Conclusion

To our knowledge, this paper provided the first evidence of small-world properties and degree distribution in large-scale anatomical networks in the human brain by means of cortical thickness measurements from MRI. These findings are largely compatible with previous human brain functional networks studies, thus significantly enhancing our understanding of how brain functional states emerge from their underlying structural substrates. Our results indicate that the morphometry-based approach we use here may be useful to reveal the patterns of anatomical connectivity in the human brain, which opens a new window for mechanistic modeling and interpretation of human brain anatomical networks recently sparked as the human connectome (Sporns et al. 2005). Further work could be conducted to examine whether these networks properties are altered during normal development and aging as well as under specific brain disorders.

Supplementary Material

Supplementary material can be found at: http://www.cercor.oxfordjournals.org/.

Notes

The authors would like to thank Dr Pedro Rosa and Jurgen Germann for their valuable comments regarding the manuscript. This work was supported by Human Brain Project grant PO1MHO52176-11 (ICBM, P.I. Dr John Mazziotta), Canadian Institutes of Health Research grant MOP-34996, and the Killam Foundation. Yong He was supported by a Jeanne Timmins Costello Fellowship of the Montreal Neurological Institute. *Conflict of Interest*: None declared.

Address correspondence to Dr Alan C. Evans, McConnell Brain Imaging Centre, Montreal Neurological Institute, 3801 University Street, Montreal, QC, Canada H3A 2B4. Email: alan.evans@mcgill.ca.

References

Achard S, Salvador R, Whitcher B, Suckling J, Bullmore E. 2006. A resilient, low-frequency, small-world human brain functional network with highly connected association cortical hubs. J Neurosci. 26:63–72.

Albert R, Jeong H, Barabasi AL. 2000. Error and attack tolerance of complex networks. Nature. 406:378–382.

Amaral LA, Scala A, Barthelemy M, Stanley HE. 2000. Classes of small-world networks. Proc Natl Acad Sci USA. 97:11149–11152.

Andrews TJ, Halpern SD, Purves D. 1997. Correlated size variations in human visual cortex, lateral geniculate nucleus, and optic tract. J Neurosci. 17:2859–2868.

Barrat A, Barthelemy M, Pastor-Satorras R, Vespignani A. 2004. The architecture of complex weighted networks. Proc Natl Acad Sci USA. 101:3747–3752.

Batagelj V, Mrvar A. 1998. Pajek—program for large network analysis. Connections. 21:47–57.

Bullmore ET, Woodruff PW, Wright IC, Rabe-Hesketh S, Howard RJ, Shuriquie N, Murray RM. 1998. Does dysplasia cause anatomical dysconnectivity in schizophrenia? Schizophr Res. 30:127–135.

Collins DL, Holmes CJ, Peters TM, Evanc AC. 1995. Automatic 3D model-based neuroanatomical segmentation. Hum Brain Mapp. 33:190–208.

Collins DL, Neelin P, Peters TM, Evans AC. 1994. Automatic 3D intersubject registration of MR volumetric data in standardized Talairach space. J Comput Assist Tomogr. 18:192–205.

Crick F, Jones E. 1993. Backwardness of human neuroanatomy. Nature. 361:109–110.

Dougherty RF, Ben-Shachar M, Bammer R, Brewer AA, Wandell BA. 2005. Functional organization of human occipital-callosal fiber tracts. Proc Natl Acad Sci USA. 102:7350–7355.

Draganski B, Gaser C, Busch V, Schuierer G, Bogdahn U, May A. 2004. Neuroplasticity: changes in gray matter induced by training. Nature. 427:311–312.

Eguiluz VM, Chialvo DR, Cecchi GA, Baliki M, Apkarian AV. 2005. Scale free brain functional networks. Phys Rev Lett. 94:018102.

Ferrer I, Blanco R, Carulla M, Condom M, Alcantara S, Olive M, Planas A. 1995. Transforming growth factor-alpha immunoreactivity in the developing adult brain. Neuroscience. 66:189–199.

Genovese CR, Lazar NA, Nichols T. 2002. Thresholding of statistical maps in functional neuroimaging using the false discovery rate. Neuroimage. 15:870–878.

Han X, Jovicich J, Salat D, van der KA, Quinn B, Czanner S, Busa E, Pacheco J, Albert M, Killiany R, et al. 2006. Reliability of MRI-derived measurements of human cerebral cortical thickness: the effects of field strength, scanner upgrade and manufacturer. Neuroimage. 32:180–194.

Hilgetag CC, Barbas H. 2006. Role of mechanical factors in the morphology of the primate cerebral cortex. PLoS Comput Biol. 2:e22.

Hilgetag CC, Burns GAPC, O'Neill MA, Scannell JW, Young MP. 2000. Anatomical connectivity defines the organization of clusters of cortical areas in the macaque monkey and the cat. Philos Trans R Soc Lond B Biol Sci. 355:91–110.

Hofer S, Frahm J. 2006. Topography of the human corpus callosum revisited—comprehensive fiber tractography using diffusion tensor magnetic resonance imaging. Neuroimage. 32:989–994.

Huang H, Zhang J, Jiang H, Wakana S, Poetscher L, Miller MI, van Zijl PC, Hillis AE, Wytik R, Mori S. 2005. DTI tractography based parcellation of white matter: application to the mid-sagittal morphology of corpus callosum. Neuroimage. 26:195–205.

Humphries MD, Gurney K, Prescott TJ. 2005. The brainstem reticular formation is a small world, not scale-free, network. Proc R Soc Lond B Biol Sci. 273:503–511.

Jiang T, He Y, Zang Y, Weng X. 2004. Modulation of functional connectivity during the resting state and the motor task. Hum Brain Mapp. 22:63–71.

Kabani N, Le GG, MacDonald D, Evans AC. 2001. Measurement of cortical thickness using an automated 3-D algorithm: a validation study. Neuroimage. 13:375–380.

Kaiser M, Hilgetag CC. 2004. Modelling the development of cortical networks. Neurocomputing. 58–60:297–302.

Kamada T, Kawai S. 1989. An algorithm for drawing general undirected graphs. Inform Process Lett. 31:7–15.

Kim JS, Singh V, Lee JK, Lerch J, Ad-Dab'bagh Y, MacDonald D, Lee JM, Kim SI, Evans AC. 2005. Automated 3-D extraction and evaluation of the inner and outer cortical surfaces using a Laplacian map and partial volume effect classification. Neuroimage. 27:210–221.

Lacquaniti F, Guigon E, Bianchi L, Ferraina S, Caminiti R. 1995. Representing spatial information for limb movement: role of area 5 in the monkey. Cereb Cortex. 5:391–409.

Lee JK, Lee JM, Kim JS, Kim IY, Evans AC, Kim SI. 2006. A novel quantitative cross-validation of different cortical surface reconstruction algorithms using MRI phantom. Neuroimage. 31:572–584.

Lerch JP, Evans AC. 2005. Cortical thickness analysis examined through power analysis and a population simulation. Neuroimage. 24:163–173.

Lerch JP, Pruessner JC, Zijdenbos A, Hampel H, Teipel SJ, Evans AC. 2005. Focal decline of cortical thickness in Alzheimer's disease identified by computational neuroanatomy. Cereb Cortex. 15:995–1001.

Lerch JP, Worsley K, Shaw WP, Greenstein DK, Lenroot RK, Giedd J, Evans AC. 2006. Mapping anatomical correlations across cerebral cortex (MACACC) using cortical thickness from MRI. Neuroimage. 31:993–1003.

MacDonald D, Kabani N, Avis D, Evans AC. 2000. Automated 3-D extraction of inner and outer surfaces of cerebral cortex from MRI. Neuroimage. 12:340–356.

Maguire EA, Gadian DG, Johnsrude IS, Good CD, Ashburner J, Frackowiak RS, Frith CD. 2000. Navigation-related structural change in the hippocampi of taxi drivers. Proc Natl Acad Sci USA. 97:4398–4403.

Makris N, Kennedy DN, McInerney S, Sorensen AG, Wang R, Caviness VS Jr, Pandya DN. 2005. Segmentation of subcomponents within the superior longitudinal fascicle in humans: a quantitative, in vivo, DT-MRI study. Cereb Cortex. 15:854–869.

Maslov S, Sneppen K. 2002. Specificity and stability in topology of protein networks. Science. 296:910–913.
Mazziotta J, Toga A, Evans A, Fox P, Lancaster J, Zilles K, Woods R, Paus T, Simpson G, Pike B, et al. 2001. A probabilistic atlas and reference system for the human brain: International Consortium for Brain Mapping (ICBM). Philos Trans R Soc Lond B Biol Sci. 356: 1293–1322.
Mechelli A, Crinion JT, Noppeney U, O'Doherty J, Ashburner J, Frackowiak RS, Price CJ. 2004. Neurolinguistics: structural plasticity in the bilingual brain. Nature. 431:757.
Mechelli A, Friston KJ, Frackowiak RS, Price CJ. 2005. Structural covariance in the human cortex. J Neurosci. 25:8303–8310.
Micheloyannis S, Pachou E, Stam CJ, Vourkas M, Erimaki S, Tsirka V. 2006. Using graph theoretical analysis of multi channel EEG to evaluate the neural efficiency hypothesis. Neurosci Lett. 402:273–277.
Milo R, Shen-Orr S, Itzkovitz S, Kashtan N, Chklovskii D, Alon U. 2002. Network motifs: simple building blocks of complex networks. Science. 298:824–827.
Mitelman SA, Buchsbaum MS, Brickman AM, Shihabuddin L. 2005. Cortical intercorrelations of frontal area volumes in schizophrenia. Neuroimage. 27:753–770.
Mountcastle VB, Lynch JC, Georgopoulos A, Sakata H, Acuna C. 1975. Posterior parietal association cortex of the monkey: command functions for operations in extrapersonal space. J Neurophysiol. 38:871–908.
Narr KL, Bilder RM, Toga AW, Woods RP, Rex DE, Szeszko PR, Robinson D, Sevy S, Gunduz-Bruce H, Wang YP, et al. 2005. Mapping cortical thickness and gray matter concentration in first episode schizophrenia. Cereb Cortex. 15:708–719.
Parent A, Carpenter MB. 1995. Human neuroanatomy. Baltimore, MD: Williams & Wilkins.
Parker GJ, Luzzi S, Alexander DC, Wheeler-Kingshott CA, Ciccarelli O, Lambon Ralph MA. 2005. Lateralization of ventral and dorsal auditory-language pathways in the human brain. Neuroimage. 24:656–666.
Penny WD, Stephan KE, Mechelli A, Friston KJ. 2004. Comparing dynamic causal models. Neuroimage. 22:1157–1172.
Petrides M. 2005. Lateral prefrontal cortex: architectonic and functional organization. Philos Trans R Soc Lond B Biol Sci. 2005:781–795.
Robbins S, Evans AC, Collins DL, Whitesides S. 2004. Tuning and comparing spatial normalization methods. Med Image Anal. 8:311–323.
Salvador R, Suckling J, Coleman MR, Pickard JD, Menon D, Bullmore E. 2005. Neurophysiological architecture of functional magnetic resonance images of human brain. Cereb Cortex. 15:1332–1342.
Salvador R, Suckling J, Schwarzbauer C, Bullmore E. 2005. Undirected graphs of frequency-dependent functional connectivity in whole brain networks. Philos Trans R Soc Lond B Biol Sci. 360: 937–946.
Shaw P, Greenstein D, Lerch J, Clasen L, Lenroot R, Gogtay N, Evans A, Rapoport J, Giedd J. 2006. Intellectual ability and cortical development in children and adolescents. Nature. 440:676–679.
Sled JG, Zijdenbos AP, Evans AC. 1998. A nonparametric method for automatic correction of intensity nonuniformity in MRI data. IEEE Trans Med Imaging. 17:87–97.
Sporns O, Chialvo DR, Kaiser M, Hilgetag CC. 2004. Organization, development and function of complex brain networks. Trends Cogn Sci. 8:418–425.
Sporns O, Tononi G. 2002. Classes of network connectivity and dynamics. Complexity. 7:28–38.
Sporns O, Tononi G, Edelman GM. 2000. Theoretical neuroanatomy: relating anatomical and functional connectivity in graphs and cortical connection matrices. Cereb Cortex. 10:127–141.
Sporns O, Tononi G, Kotter R. 2005. The human connectome: a structural description of the human brain. PLoS Comput Biol. 1:e42.
Sporns O, Zwi JD. 2004. The small world of the cerebral cortex. Neuroinformatics. 2:145–162.
Stam CJ. 2004. Functional connectivity patterns of human magnetoencephalographic recordings: a 'small-world' network? Neurosci Lett. 355:25–28.
Stam CJ, Jones BF, Nolte G, Breakspear M, Scheltens P. 2007. Small-world networks and functional connectivity in Alzheimer's disease. Cereb Cortex. 17:92–99.
Steinmetz H, Herzog A, Huang Y, Hacklander T. 1994. Discordant brainsurface anatomy in monozygotic twins. N Engl J Med. 331:951–952.
Stephan KE, Hilgetag CC, Burns GA, O'Neill MA, Young MP, Kotter R. 2000. Computational analysis of functional connectivity between areas of primate cerebral cortex. Philos Trans R Soc Lond B Biol Sci. 355:111–126.
Stephan KE, Kamper L, Bozkurt A, Burns GA, Young MP, Kotter R. 2001. Advanced database methodology for the collation of connectivity data on the Macaque brain (CoCoMac). Philos Trans R Soc Lond B Biol Sci. 356:1159–1186.
Strogatz SH. 2001. Exploring complex networks. Nature. 410:268–276.
Suddath RL, Christison GW, Torrey EF, Casanova MF, Weinberger DR. 1990. Anatomical abnormalities in the brains of monozygotic twins discordant for schizophrenia. N Engl J Med. 322:789–794.
Talairach J, Tournoux P. 1988. Co-planar stereotaxic atlas of the human brain. New York: Thieme.
Thompson PM, Cannon TD, Narr KL, van Erp T, Poutanen VP, Huttunen M, Lonnqvist J, Standertskjold-Nordenstam CG, Kaprio J, Khaledy M, et al. 2001. Genetic influences on brain structure. Nat Neurosci. 4:1253–1258.
Toga AW, Thompson PM. 2003. Mapping brain asymmetry. Nat Rev Neurosci. 4:37–48.
Tononi G, Edelman GM, Sporns O. 1998. Complexity and coherency: integrating information in the brain. Trends Cogn Sci. 2:474–484.
Tononi G, Sporns O, Edelman GM. 1994. A measure for brain complexity: relating functional segregation and integration in the nervous system. Proc Natl Acad Sci USA. 91:5033–5037.
Tootell RB, Tsao D, Vanduffel W. 2003. Neuroimaging weighs in: humans meet macaques in "primate" visual cortex. J Neurosci. 23:3981–3989.
Tuch DS, Wisco JJ, Khachaturian MH, Ekstrom LB, Kotter R, Vanduffel W. 2005. Q-ball imaging of macaque white matter architecture. Philos Trans R Soc Lond B Biol Sci. 360:869–879.
Wakana S, Jiang H, Nagae-Poetscher LM, van Zijl PC, Mori S. 2004. Fiber tract-based atlas of human white matter anatomy. Radiology. 2003:77–87.
Watkins KE, Paus T, Lerch JP, Zijdenbos A, Collins DL, Neelin P, Taylor J, Worsley KJ, Evans AC. 2001. Structural asymmetries in the human brain: a voxel-based statistical analysis of 142 MRI scans. Cereb Cortex. 11:868–877.
Watts DJ, Strogatz SH. 1998. Collective dynamics of 'small-world' networks. Nature. 393:440–442.
Woodruff PW, Wright IC, Shuriquie N, Russouw H, Rushe T, Howard RJ, Graves M, Bullmore ET, Murray RM. 1997. Structural brain abnormalities in male schizophrenics reflect fronto-temporal dissociation. Psychol Med. 27:1257–1266.
Worsley KJ, Chen JI, Lerch J, Evans AC. 2005. Comparing functional connectivity via thresholding correlations and singular value decomposition. Philos Trans R Soc Lond B Biol Sci. 360:913–920.
Wright IC, Sharma T, Ellison ZR, McGuire PK, Friston KJ, Brammer MJ, Murray RM, Bullmore ET. 1999. Supra-regional brain systems and the neuropathology of schizophrenia. Cereb Cortex. 9:366–378.
Zarei M, Johansen-Berg H, Smith S, Ciccarelli O, Thompson AJ, Matthews PM. 2006. Functional anatomy of interhemispheric cortical connections in the human brain. J Anat. 209:311–320.
Zijdenbos AP, Forghani R, Evans AC. 2002. Automatic "pipeline" analysis of 3-D MRI data for clinical trials: application to multiple sclerosis. IEEE Trans Med Imaging. 21:1280–1291.